IEEE Access
Multidisciplinary | Rapid Review | Open Access Journal

Received April 12, 2019, accepted April 16, 2019, date of publication April 22, 2019, date of current version May 1, 2019.

Digital Object Identifier 10.1109/ACCESS.2019.2912449

Influence of Non-Ideal Factors on the Boundary Control of Buck Converters With Curved Switching Surfaces

JINGHAO LI AND AIGUO WU
School of Electrical and Information Engineering, Tianjin University, Tianjin 300072, China
Corresponding author: Jinghao Li (lijinghao@tju.edu.cn)

ABSTRACT In boundary control for Buck converters, the dynamic behavior characteristics are strongly influenced by some non-ideal factors. This influence is detailedly analyzed in this paper, and some design principles of the switching surface (SS) are proposed accordingly. First, by using the Adomian decomposition method, a general expression which can approximate the theoretically time-optimal SS with different degrees is obtained, and it can be seen as an extension of the existing second-order SSs. Second, the influences of load resistance, the ratio of capacitance and inductance, parasitic parameters, and the truncation order of SS are respectively shown by analyzing the behavior characteristics of the points along the SSs. For a specific SS, it is shown that the light load and low ratio of capacitance and inductance may cause overshoot of output voltage, which should be avoided in practical application. The simulation and experimental results are provided to confirm the correctness of theoretical analyses, which can give some instructions to determine the SS coefficients in the application of boundary control.

INDEX TERMS Boundary control, switching surface, time optimal control (TOC), buck converter, non-ideal factors.

I. INTRODUCTION

With the wide application of DC-DC power converters in different occasions, including renewable power generation, electric vehicle, consumer electronics and so on, further improving their dynamic performance by advanced control method has attracted many interests. Boundary control is a geometrically-based control method, which is suitable for time-varying structure systems like switching converters [1], [2]. The basic strategy of boundary control is using a switching surface (SS), which is a straight or curved line in state-plane, to decide the switching action. Take the case of a Buck converter, it is operated in turn-on mode on one side of the SS and turn-off mode on the other side (to avoid chatter, it is necessary to set a hysteresis in sliding-mode motion). Currently, the boundary control has been used in different DC-DC converters [3]–[22]. Depending on the SSs in state-plane, different boundary control methods have been proposed. The controller with a first-order SS, which is a straight line passing through the desired point, was discussed in [3]–[5]. Compared with the traditional linear control techniques, this sliding-mode strategy generally provides improved dynamic response and robustness, but the transient process is not time-optimal. According to Pontryagin's minimum principle, the optimal SS is the natural state-plane trajectory passing through the target operating point, and only one switching action is required during the time-optimal transient process. Obviously, the time optimal control (TOC) can be seen as a special form of boundary control. An accurate analytic expression of the optimal SS for Buck converters has been given in [11]. However, it only copes with the zero or constant current load. For the case of resistive load, it is difficult to eliminate the time variable in state-plane trajectory, so obtaining the analytic optimal SS is almost impossible. To solve this problem, some curved SSs have been proposed to approximate the optimal SS, including the second-order SS [8], unloaded SS [11], and high-order SS [23]. Particularly, the second-order SS, which gives a simple switching law for a better dynamic response than first-order SS [9], [10], has attracted significant attention and been applied in many different topologies [22]–[32]. Since the changing switching frequency makes it difficult to

The associate editor coordinating the review of this manuscript and approving it for publication was Ning Sun.

determine the filter parameters, a fixed-frequency approach with the second-order SS was proposed in [17] to minimize the frequency variation. There is also a hybrid method combining the second-order SS control and traditional PWM strategy to obtain a constant switching frequency presented in [20].

Although the second-order SS has been widely used successfully, all the existing researches only concentrate on the ideal application condition, which assumes that the true values of converter parameters are exactly equal to the rated values used in SS coefficients. In fact, the practical non-idealities, such as parametric variations or parasitic parameters, will significantly influence the large-signal behavior characteristics of the system, and these effects can be either positive or negative. How the non-ideal factors affect the dynamic performance of the system is worth researching in depth. Furthermore, the influence of deviations between the practical SS and the ideal one is also need to be considered. Up to now, there is still no systematic research on these problems.

In this paper, the influence of non-ideal factors on the boundary control of Buck converters is detailedly analysed, and some design principles of the SS are provided. Firstly, for the convenience of researching the dynamic performance provided by curved SSs with different coefficients and orders, a general expression of SSs is derived by solving the state-plane trajectory equations directly using the Adomian decomposition method (ADM). Differing from the existing SSs, this expression is universal. With different truncation orders, a series of SSs with different approach degrees to the time-optimal SS can be obtained. Thus, this expression can be seen as an extension of the existing second-order SSs. Secondly, considering practical non-ideal factors, including parameter deviations of load and output filter, parasitic parameters, and deviations from the ideal SS, the large-signal behavior characteristics of boundary control are analysed. It is shown that, for a specific SS, the light load and low ratio of filter capacitance and inductance may cause an overshoot of output voltage, and the parasitic resistances of output filter will enlarge the sliding-mode region generally. Simulation and experimental results of the boundary control with different SS coefficients and circuit parameters are presented to validate the correctness of the above theoretical analyses.

This paper is organized as follows. In Section II, a general expression of the curved SSs is obtained by using the ADM. Then, the large-signal behavior characteristics analyses, containing the analyses of several non-ideal factors, are given in Section III. Experimental results are presented in Section IV and the conclusions are presented in Section V.

II. DERIVATION OF THE GENERAL EXPRESSION OF CURVED SWITCHING SURFACES

In this section, we provide a general expression which can approximate the theoretically time-optimal SS with different degrees. For ease of understanding the derivation process, the ADM is briefly introduced firstly.

A. ADOMIAN DECOMPOSITION METHOD

The ADM can provide an analytical approximation solution to a rather wide class of nonlinear equations without linearization, so it has been widely used in the applied sciences and engineering [33], [34]. This method is suitable for solving an initial value problem of the nonlinear differential equations in the following form

$$Lu + Ru + Nu = g \tag{1}$$

where L is an invertible linear operator, R is the linear remainder operator, g and u are the system input and output respectively, and Nu is the nonlinear part of the system. Solving for u yields

$$u = u(0) + L^{-1}g - L^{-1}Ru - L^{-1}Nu \tag{2}$$

The nonlinear term Nu will be decomposed to a infinite series

$$Nu = \sum_{n=0}^{\infty} A_n \tag{3}$$

where A_n are called Adomian polynomials, and u will also be decomposed to a series which leads to

$$\sum_{n=0}^{\infty} u_n = u(0) + L^{-1}g - L^{-1}R\sum_{n=0}^{\infty} u_n - L^{-1}\sum_{n=0}^{\infty} A_n \tag{4}$$

Then, we can get

$$\begin{aligned} u_0 &= u(0) + L^{-1}g \\ u_1 &= -L^{-1}Ru_0 - L^{-1}A_0 \\ &\vdots \\ u_{n+1} &= -L^{-1}Ru_n - L^{-1}A_n \end{aligned} \tag{5}$$

The Adomian polynomials are defined by the following formula [35]

$$A_n = \frac{1}{n!}\frac{\partial^n}{\partial \lambda^n}[F(u(\lambda))]_{\lambda=0} \tag{6}$$

where $F(u) \equiv Nu$, λ is a parameter for collecting terms, and

$$u(\lambda) = \sum_{i=0}^{\infty} u_i \lambda^i \tag{7}$$

Thus, the first several Adomian polynomials are given by

$$\begin{aligned} A_0 &= F(u_0) \\ A_1 &= u_1 F'(u_0) \\ A_2 &= u_2 F'(u_0) + (u_1^2/2!)F''(u_0) \\ A_3 &= u_3 F'(u_0) + u_1 u_2 F''(u_0) + (u_1^3/3!)F^{(3)}(u_0) \\ &\vdots \end{aligned} \tag{8}$$

In an attempt to improve the convergence rate and accuracy, some researchers have developed modifications to the ADM. In [36], under an assumption that the function $f \equiv u(0) + L^{-1}g$ can be divided into two parts, namely f_1 and f_2, a variation on the components u_0 and u_1 is proposed.

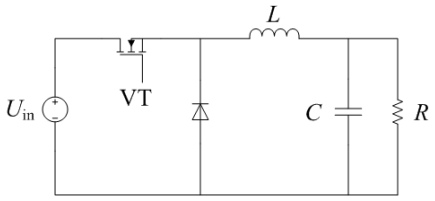

FIGURE 1. The circuit diagram of buck converters.

In this method, the recursive algorithm of the solution is given by

$$\begin{aligned} u_0 &= f_1 \\ u_1 &= f_2 - L^{-1}Ru_0 - L^{-1}A_0 \\ &\vdots \\ u_{n+1} &= -L^{-1}Ru_n - L^{-1}A_n \end{aligned} \tag{9}$$

As stated in [36], the success of this method mainly depends on the selection of f_1 and f_2. By an appropriate selection, it will accelerate the convergence and reduce computational work greatly. This will also be verified in this paper.

B. DERIVATION OF THE GENERAL EXPRESSION OF CURVED SWITCHING SURFACES

The circuit diagram of a basic Buck converter is shown in Fig.1. To simplify analysis, the parasitic elements are neglected for the moment. Considering continuous conduction mode (CCM) operation, the state space equation describing Buck converters can be expressed as

$$\begin{bmatrix} \dot{i}_c \\ \dot{u}_o \end{bmatrix} = \begin{bmatrix} -1/RC & -1/L \\ 1/C & 0 \end{bmatrix} \begin{bmatrix} i_c \\ u_o \end{bmatrix} + \begin{bmatrix} sU_{in}/L - (1-s)U_D/L \\ 0 \end{bmatrix} \tag{10}$$

where R, L, and C represent the load resistance, inductance, and capacitance, respectively; U_{in} represents input voltage; U_D represents the forward voltage drop of freewheeling diode; u_o represents the output voltage; and $s = 0$ or 1 is the switching state of the power switch. The main control objective of Buck converters is to achieve a quick adjustment of output voltage to a reference value U_{ref}.

The state-plane trajectories of Buck converters are shown in Fig.2. These trajectories are obtained by solving (10) numerically ($s = 0$ or 1), with different initial values and the parameters listed in Table 1. According to the minimum-time principle, the optimum SS, denoted by σ^i, should consist of the trajectories passing through the target operating point $(U_{ref}, 0)$. Specifically, the part of σ^i with $i_c > 0$ is set along with the off-state trajectory, and the part with $i_c < 0$ is set along with the on-state trajectory. In order to achieve the time-optimal response, the switch VT should be set to off when the state is on the right side of σ^i and be set to on when the state is on the left side of σ^i. When the state reaches σ^i, the VT switches, and the state will move towards target operating point. Only one switching action is required

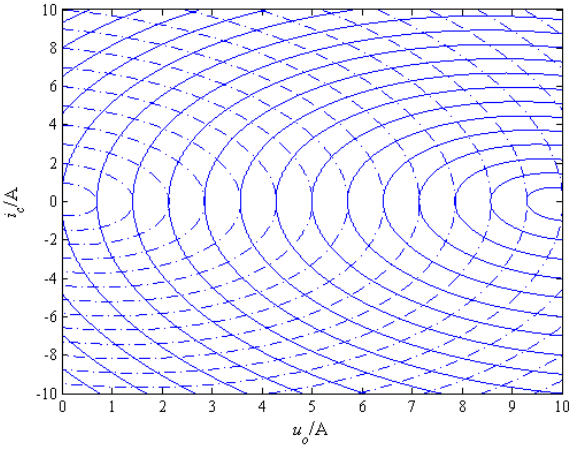

FIGURE 2. The state plane trajectories of a buck converter.

TABLE 1. Parameters of the buck converter.

Parameter	Value
U_{in}	$10V$
L	$330\mu H$
C	$480\mu F$
Z_C	$0.5\sqrt{L/C}$
R	$10Z_C$
U_{ref}	$5V$

during the transient process. Thus it can be seen that the key to realizing TOC is obtaining an accurate expression of σ^i.

In order to obtain the expression of optimum SS for TOC, rewrite (10) into the following equation

$$\dot{u}_o \frac{d\dot{u}_o}{du_o} + \frac{\dot{u}_o}{RC} + \frac{u_o}{LC} = \frac{sU_{in} - (1-s)U_D}{LC} \tag{11}$$

Equation (11) contains a product of $\dot{u}_o$ and $\frac{d\dot{u}_o}{du_o}$. It can't be solved by the ADM directly, so a variable substitution will be used. Define

$$\begin{cases} y = \frac{1}{2}\dot{u}_o^2 \\ x = u_o \end{cases} \tag{12}$$

In the following part, the criteria for switching off and on will be discussed respectively.

1) THE SWITCHING SURFACE FOR OFF-STATE

As discussed above, the part of σ^i on the off-state trajectory is above the zero-axis. Considering $\dot{u}_o > 0$, it can be seen that

$$\dot{u}_o = \sqrt{2y} \tag{13}$$

Thus, with $s = 0$, (11) can be transformed into

$$\frac{dy}{dx} = -\frac{U_D}{LC} - \frac{1}{LC}x - \frac{\sqrt{2}}{RC}\sqrt{y} \tag{14}$$

Equation (14) is a nonlinear non-autonomous differential equation. The problem can be summed up as solving (14) with the initial condition

$$y(U_{ref}) = 0 \tag{15}$$

According to the Adomian decomposition method, applying the integral operator to both sides of (14) yields

$$y = y(U_{ref}) - \frac{U_D}{LC}(x - U_{ref}) - \frac{1}{2LC}(x^2 - U_{ref}^2) - \sum_{n=0}^{\infty} \int_{U_{ref}}^{x} A_n dx \tag{16}$$

where the A_n are the appropriate polynomials for $Ny = \frac{\sqrt{2y}}{RC}$. They are given by

$$\begin{aligned} A_0 &= \frac{\sqrt{2}}{RC}\sqrt{y_0} \\ A_1 &= \frac{\sqrt{2}}{RC}\frac{y_1}{2\sqrt{y_0}} \\ A_2 &= \frac{\sqrt{2}}{RC}(\frac{y_2}{2\sqrt{y_0}} - \frac{y_1^2}{8y_0^{1.5}}) \\ &\vdots \end{aligned} \tag{17}$$

If using the standard algorithm given by (5), the calculation will be very difficult due to the integral of irrational function. To avoid this, the modified technique is used. Firstly, divide the function f into two parts. We select

$$\begin{aligned} f_1 &= \frac{U_{ref}^2}{2LC} \\ f_2 &= -\frac{x^2}{2LC} \end{aligned} \tag{18}$$

Using the modified algorithm given by (9), we obtain

$$\begin{aligned} y_0 &= \frac{U_{ref}^2}{2LC} \\ y_1 &= (-\frac{U_D}{LC} - \frac{U_{ref}}{RC\sqrt{LC}})(x - U_{ref}) - \frac{x^2}{2LC} \\ y_2 &= -(\frac{U_D}{RC\sqrt{LC}} + \frac{U_{ref}}{(RC)^2})(x - U_{ref}) \\ &\quad + (\frac{U_D}{2U_{ref}RC\sqrt{LC}} + \frac{1}{2(RC)^2})(x^2 - U_{ref}^2) \\ &\quad + \frac{1}{6U_{ref}RC\sqrt{LC}}(x^3 - U_{ref}^3) \\ &\vdots \end{aligned} \tag{19}$$

Obviously, with the modified algorithm, y can be calculated by summing a series of power functions. By continuing the calculation, a solution of (14) with arbitrary precision can be obtained. In this paper, we truncate the decomposition series after $n = 2$ and 3, then

$$y_{(2)} \approx y_0 + y_1 \tag{20}$$

$$y_{(3)} \approx y_0 + y_1 + y_2 \tag{21}$$

According to the above approximate solutions, two SSs for switching *VT* off can be obtained, which are respectively given by

For case $i_c > 0$:

$$\sigma^{A2} = i_C^2 - k_{21}(u_o - U_{ref}) - m_{21}(u_o^2 - U_{ref}^2) \tag{22}$$

$$\sigma^{A3} = i_C^2 - k_{31}(u_o - U_{ref}) - m_{31}(u_o^2 - U_{ref}^2) - n_{31}(u_o^3 - U_{ref}^3) \tag{23}$$

where $k_{21}, m_{21}, k_{31}, m_{31}$, and n_{31} are constants after the circuit parameters being determined. Considering the voltage drop of the diode is very small compared with U_{in}, for simplicity in the following sections, if not specifically mentioned, $U_D = 0$ is adopted. Thus,

$$\begin{aligned} k_{21} &= -\frac{2U_{ref}}{R}\sqrt{\frac{C}{L}}, \quad m_{21} = -\frac{C}{L}, \\ k_{31} &= -\frac{2U_{ref}}{R}(\frac{1}{R} + \sqrt{\frac{C}{L}}), \quad m_{31} = \frac{1}{R^2} - \frac{C}{L}, \\ n_{31} &= \frac{1}{3U_{ref}R}\sqrt{\frac{C}{L}}. \end{aligned} \tag{24}$$

2) THE SWITCHING SURFACE FOR ON-STATE

The part of σ^i on the on-state trajectory is below the zero-axis, so $\dot{u}_o < 0$, and

$$\dot{u}_o = -\sqrt{2y} \tag{25}$$

Thus, with $s = 1$, (11) can be transformed into

$$\frac{dy}{dx} = \frac{U_{in}}{LC} - \frac{1}{LC}x + \frac{\sqrt{2}}{RC}\sqrt{y} \tag{26}$$

The problem can be summed up as solving (26) with the initial condition (15). Applying the integral operator to both sides of (26) yields

$$y = y(U_{ref}) + \frac{U_{in}}{LC}(x - U_{ref}) - \frac{1}{2LC}(x^2 - U_{ref}^2) - \sum_{n=0}^{\infty} \int_{U_{ref}}^{x} A_n dx \tag{27}$$

where the A_n are the appropriate polynomials for $Ny = -\frac{\sqrt{2y}}{RC}$. They are given by

$$\begin{aligned} A_0 &= -\frac{\sqrt{2}}{RC}\sqrt{y_0} \\ A_1 &= -\frac{\sqrt{2}}{RC}\frac{y_1}{2\sqrt{y_0}} \\ A_2 &= -\frac{\sqrt{2}}{RC}(\frac{y_2}{2\sqrt{y_0}} - \frac{y_1^2}{8y_0^{1.5}}) \\ &\vdots \end{aligned} \tag{28}$$

It can be seen that

$$f = \frac{U_{in}}{LC}(x - U_{ref}) - \frac{1}{2LC}(x^2 - U_{ref}^2) \tag{29}$$

We select

$$\begin{aligned} f_1 &= \frac{U_{ref}^2}{2LC} \\ f_2 &= \frac{U_{in}}{LC}(x - U_{ref}) - \frac{x^2}{2LC} \end{aligned} \tag{30}$$

Using the modified algorithm given by (9), we obtain

$$\begin{aligned} y_0 &= \frac{U_{ref}^2}{2LC} \\ y_1 &= (\frac{U_{in}}{LC} + \frac{U_{ref}}{RC\sqrt{LC}})(x - U_{ref}) - \frac{x^2}{2LC} \\ y_2 &= -(\frac{U_{in}}{RC\sqrt{LC}} + \frac{U_{ref}}{(RC)^2})(x - U_{ref}) \\ &\quad + (\frac{U_{in}}{2U_{ref}RC\sqrt{LC}} + \frac{1}{2(RC)^2})(x^2 - U_{ref}^2) \\ &\quad - \frac{1}{6U_{ref}RC\sqrt{LC}}(x^3 - U_{ref}^3) \\ &\vdots \end{aligned} \tag{31}$$

Similarly, if the second- and third-order approximation solutions are adopted, the SSs for switching *VT* on are respectively given by

For case $i_c < 0$:

$$\sigma^{A2} = -i_C^2 + k_{22}(u_o - U_{ref}) + m_{22}(u_o^2 - U_{ref}^2) \tag{32}$$

$$\begin{aligned} \sigma^{A3} &= -i_C^2 + k_{32}(u_o - U_{ref}) + m_{32}(u_o^2 - U_{ref}^2) \\ &\quad + n_{32}(u_o^3 - U_{ref}^3) \end{aligned} \tag{33}$$

where k_{22}, m_{22}, k_{32}, m_{32}, and n_{32} are also constants after the circuit parameters being determined, and

$$\begin{aligned} k_{22} &= \frac{2CU_{in}}{L} + \frac{2U_{ref}}{R}\sqrt{\frac{C}{L}}, m_{22} = -\frac{C}{L}, \\ k_{32} &= \frac{2CU_{in}}{L} - \frac{2U_{in}}{R}\sqrt{\frac{C}{L}} - \frac{2U_{ref}}{R}(\frac{1}{R} - \sqrt{\frac{C}{L}}) \\ m_{32} &= \frac{1}{R^2} - \frac{C}{L} + \frac{U_{in}}{U_{ref}R}\sqrt{\frac{C}{L}}, \\ n_{32} &= -\frac{1}{3U_{ref}R}\sqrt{\frac{C}{L}}. \end{aligned} \tag{34}$$

3) CONTROL LAW

Based on the above analyses, the boundary control law is

$$\begin{aligned} &\text{Case I:} i_c > 0 \\ &\quad \text{if } \sigma^{Ai} > 0, \text{ then } s = 0, \text{ else } s = 1; \\ &\text{Case II: } i_c < 0 \\ &\quad \text{if } \sigma^{Ai} < 0, \text{ then } s = 1, \text{ else } s = 0; \end{aligned} \tag{35}$$

where $i = 2, 3$. To avoid an excessively high switching frequency, a hysteresis or minimum switching time interval should be set in the application of this control law.

C. COMPARISONS OF DIFFERENT SWITCHING SURFACES

According to (19) and (31), a general expression to approximate the time-optimal SS can be given by (36), as shown at the bottom of the next page, where n indicates the truncation order. Without loss of generality, the state variables can be normalized as follows:

$$u_{on} = \frac{u_o}{U_{ref}}, \quad i_{Cn} = i_C\frac{Z_C}{U_{ref}} \tag{37}$$

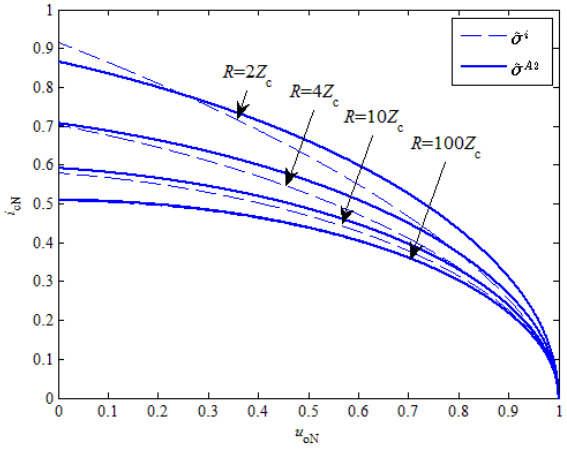

(a)

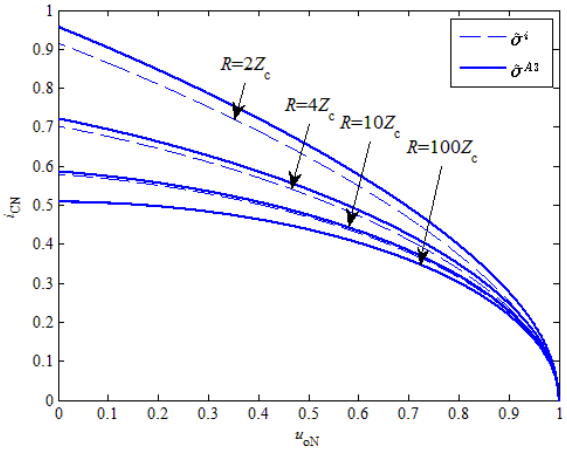

(b)

FIGURE 3. Comparisons of σ^i, σ^{A2} and σ^{A3} ($s = 0$). (a) σ^i and σ^{A2}. (b) σ^i and σ^{A3}.

where $Z_C = \frac{1}{2}\sqrt{\frac{L}{C}}$. Putting (37) into the reversed system of (10), and solving it numerically with the initial condition $u_{on}(0) = 1$, $i_{Cn}(0) = 0$, the normalized time-optimal switching surface $\hat{\sigma}^i$ can be obtained. The normalized SSs corresponding to (22) and (23), denoted by $\hat{\sigma}^{A2}$ and $\hat{\sigma}^{A3}$ respectively, can be obtained by putting (37) into (24). In Fig.3, a comparison of $\hat{\sigma}^i$, $\hat{\sigma}^{A2}$ and $\hat{\sigma}^{A3}$ is shown.

As can be seen from Fig.3, with the truncation order increasing, the SS will be closer to the time-optimal one. Equation (22) and (32) give an extension of traditional second-order SSs [8], [11], which are used mostly in the existing researches. In particular, the unloaded SS in [11] is equivalent to (22) and (32) in the case of $R \to +\infty$. By adjusting the parameter R in the coefficients, the SS can be closer to the optimal one.

Fig.4 shows the simulation results in time-domain with σ^{A2} and σ^{A3}, including output voltage (u_o), inductor current (i_L), and the gate signal to VT. The circuit parameters are given in Table 1. It can be seen that the output voltage

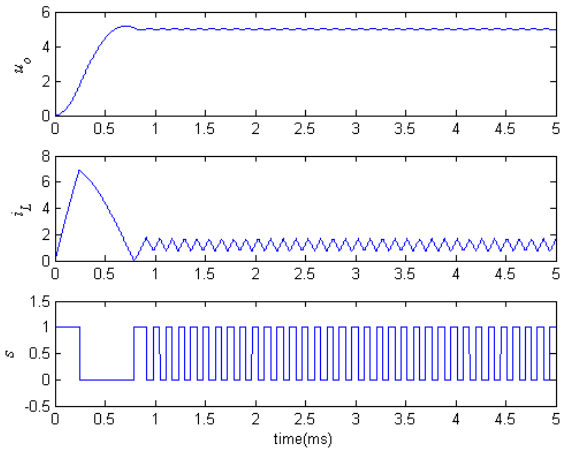

(a)

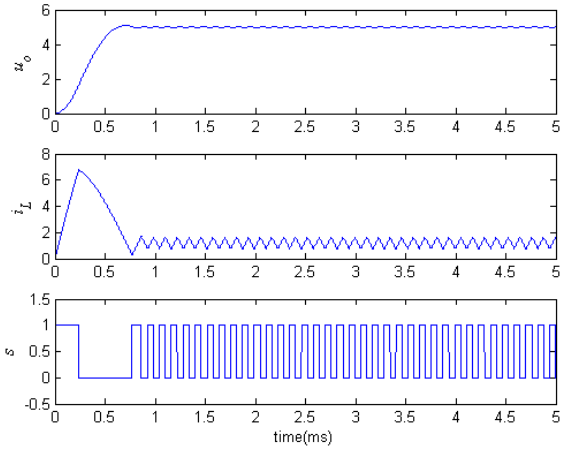

(b)

FIGURE 4. Simulation waveforms in time-domain with σ^{A2} and σ^{A3}.

has a small overshoot with σ^{A2}, and has nearly no overshoot with σ^{A3}. Fig.5 shows the state trajectory corresponding to Fig.4(a). It can be seen that the system trajectory has deviated from σ^{A2} slightly. In summary, both of the SSs can be used to boundary control to obtain a time-optimal dynamic response, and σ^{A3} provides a better approximation of σ^{i}.

Ideally, the coefficients can be determined by the converter parameters directly according to (24) and (34). However, the existence of non-ideal factors is unavoidable in practical circuits. The determination of coefficients must consider the influence of them. Thus, it is necessary to analyze the large-signal behavior characteristics of the system under the influence of practical nonidealities.

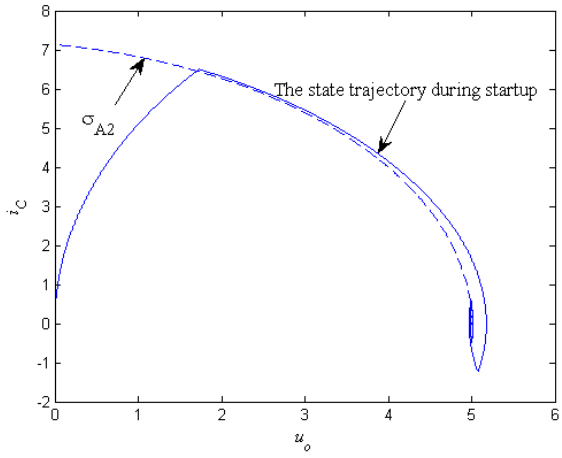

FIGURE 5. The state trajectory corresponding to Figure.4(a).

III. LARGE-SIGNAL CHARACTERISTICS ANALYSES

The points along a curved surface σ can be categorized into three types: refractive, reflective, and rejective modes. The three ones have different characteristics.

(1) Refractive Mode: In this case, the trajectories on one side of σ will approach the SS while on the other side the trajectories will be away from σ. The refractive points on one side of the SS satisfy

$$\sigma \frac{d\sigma}{dt} < 0 \tag{38}$$

and on the other side, we have

$$\sigma \frac{d\sigma}{dt} > 0 \tag{39}$$

Note that $\frac{d\sigma}{dt}$ at the two sides of the SS have a different expression because of the different switching states, similarly hereinafter.

(2) Reflective Mode: In this case, the trajectories on both sides of σ will approach the SS. The reflective points along the SS satisfy

$$\sigma \frac{d\sigma}{dt} < 0 \tag{40}$$

When reflective mode occurs, the state variables of the converter will move along the SS. It is equivalent to sliding-mode control in this case.

(3) Rejective Mode: In this case, the trajectories on both sides of σ will be away from the SS. The rejective points along the SS satisfy

$$\sigma \frac{d\sigma}{dt} > 0 \tag{41}$$

Thus, the type of points along σ can be ascertained according to the sign of σ and $\frac{d\sigma}{dt}$.

$$\sigma^{An} = \begin{cases} i_C^2 - k_{n1}(u_o - U_{ref}) - m_{n1}(u_o^2 - U_{ref}^2) - n_{n1}(u_o^3 - U_{ref}^3) - \cdots, i_C > 0 \\ -i_C^2 + k_{n2}(u_o - U_{ref}) + m_{n2}(u_o^2 - U_{ref}^2) + n_{n2}(u_o^3 - U_{ref}^3) + \cdots, i_C < 0 \end{cases} \tag{36}$$

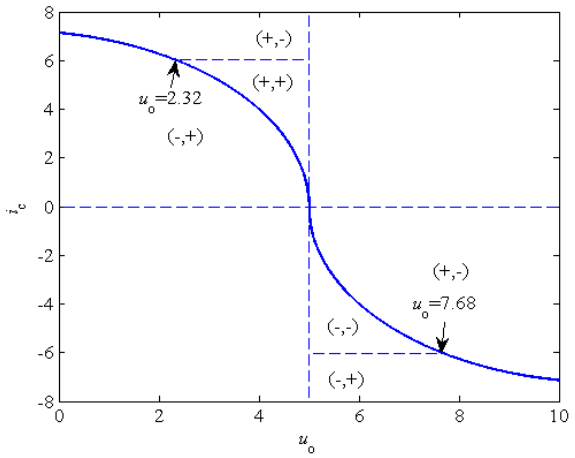

FIGURE 6. The boundary of the regions having different characteristics(σ^{A2}).

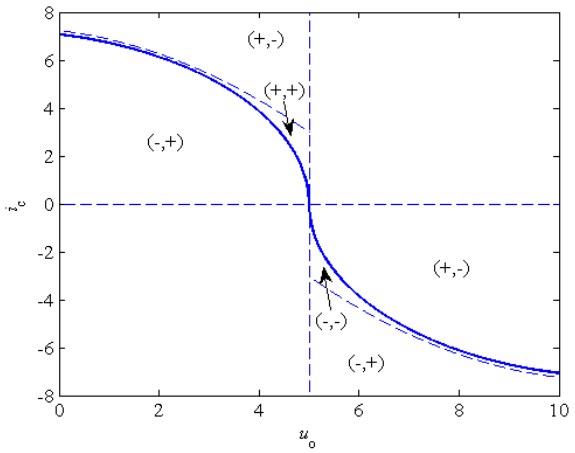

FIGURE 7. The boundary of the regions having different characteristics(σ^{A3}).

A. THE IDEAL CASE

Firstly, we suppose that the model structure given by (10) and converter parameters are accurate. For σ^{A2}, the derivative versus time of the SS is given by (42). By substituting (10) into (42), equation (43) can be obtained, as shown at the bottom of this page.

Note that, in the calculation of $\frac{d\sigma}{dt}$, the value of s depends on the position of the concerned point, which is above or below the SS. Curves $\sigma^{A2}=0$ and $\frac{d\sigma^{A2}}{dt}=0$ form the boundary of the regions which have different behavior characteristics. With the nominal parameters given in Table 1, the graphs of these boundary curves are shown in Fig.6.

In Fig.6, the sign of σ^{A2} and $\frac{d\sigma^{A2}}{dt}$ in different regions are given in parentheses. The first sign is corresponding to σ and the second sign is corresponding to $\frac{d\sigma}{dt}$ (e.g., "$(+,-)$" indicates $\sigma>0$ and $\frac{d\sigma}{dt}<0$ in this region). According to Fig.5, when $u_o<2.32$ or $u_o>7.68$, the points along σ^{A2} are reflective; when $2.32<u_o<7.68$, the points along σ^{A2} are refractive. It means that when the state point hit the SS in the interval $[2.32, 7.68]$, it will not move along the SS strictly, and the deviation degree depends on the error between the SS and the natural trajectory; if the intersection point is outside the interval, the state point will move along the SS with hysteretic switching actions for some time until it enters the refractive region.

Similarly, the derivative versus time of σ^{A3} can be obtained, and the regions having different behavior characteristics are illustrated in Fig.7. It can be seen that all the points along σ^{A3} are refractive. It means that wherever the state point hit the switching surface, it will not move along the SS strictly, but the SS is very close to the natural trajectory.

B. CONSIDERING PARAMETRIC VARIATIONS

In practical converters, the circuit parameters deviate from their nominal value inevitably. When considering parametric

$$\frac{d\sigma^{A2}}{dt}=\begin{cases}2i_C\dfrac{di_C}{dt}+\dfrac{2U_{ref}}{R}\sqrt{\dfrac{C}{L}}\dfrac{du_o}{dt}+\dfrac{2Cu_o}{L}\dfrac{du_o}{dt} & i_C>0\\ -2i_C\dfrac{di_C}{dt}+\left(\dfrac{2CU_{in}}{L}+\dfrac{2U_{ref}}{R}\sqrt{\dfrac{C}{L}}\right)\dfrac{du_o}{dt}-\dfrac{2Cu_o}{L}\dfrac{du_o}{dt} & i_C<0\end{cases} \tag{42}$$

$$\frac{d\sigma^{A2}}{dt}=\begin{cases}-\dfrac{2}{RC}i_C^2+\left(\dfrac{2sU_{in}}{L}+\dfrac{2U_{ref}}{R\sqrt{LC}}\right)i_C & i_C>0\\ \dfrac{2}{RC}i_C^2+\left[\dfrac{2U_{in}}{L}(1-s)+\dfrac{2U_{ref}}{R\sqrt{LC}}\right]i_C & i_C<0\end{cases} \tag{43}$$

$$\frac{d\sigma^{A2N}}{dt}=\begin{cases}-\dfrac{2}{RC}i_C^2+\left(\dfrac{2sU_{in}}{L}+\dfrac{2U_{ref}}{R_NC}\sqrt{\dfrac{C_N}{L_N}}\right)i_C+\left(\dfrac{2C_N}{CL_N}-\dfrac{2}{L}\right)u_oi_C & i_C>0\\ \dfrac{2}{RC}i_C^2+\left(\dfrac{2C_NU_{in}}{CL_N}+\dfrac{2U_{ref}}{R_NC}\sqrt{\dfrac{C_N}{L_N}}-\dfrac{2sU_{in}}{L}\right)i_C-\left(\dfrac{2C_N}{CL_N}-\dfrac{2}{L}\right)u_oi_C & i_C<0\end{cases} \tag{44}$$

$$\begin{bmatrix}\dot{i}_c\\ \dot{u}_o\end{bmatrix}=\begin{bmatrix}-\dfrac{L+R_LRC}{LC(R+R_C)} & -\dfrac{R+R_L}{L(R+R_C)}\\ \dfrac{R(L-R_LR_CC)}{LC(R+R_C)} & -\dfrac{(R+R_L)R_C}{(R+R_C)L}\end{bmatrix}\begin{bmatrix}i_C\\ u_o\end{bmatrix}+\begin{bmatrix}\dfrac{sU_{in}R-(1-s)U_DR}{L(R+R_C)}\\ \dfrac{sU_{in}RR_C-(1-s)U_DRR_C}{L(R+R_C)}\end{bmatrix} \tag{45}$$

variations, the large-signal behavior of the converter need to be reconsidered. For σ^{A2}, we substitute L_N, C_N, R_N, which denote the nominal value of inductance, capacitance and load resistance respectively, for L, C, R in (24) and (34). Correspondingly, the expression of $\frac{d\sigma^{A2}}{dt}$ is changed into (44), as shown at the bottom of the last page.

Consider a $\pm 50\%$ variation in R_N and a $\pm 20\%$ variation in C_N/L_N. The boundary curves under parametric variations are shown in Fig.8.

Fig.8(a), (b) show the boundary curves with $R_N = 1.5R, 0.5R$ respectively. It can be seen that if the nominal value of load resistance is bigger than the true value, the reflective region will be enlarged; otherwise, the refractive region will be enlarged. Fig.8(c) shows the boundary curves with $C_N/L_N = 1.2C/L$. It can be seen that the refractive region is enlarged compared with the ideal case. Fig.8(d) shows the opposite case that all the points along the switching surface are reflective with $C_N/L_N = 0.8C/L$.

For σ^{A3}, the analysis method is the same. Fig.9(a), (b) show the boundary curves with $R_N = 1.5R, 0.5R$ respectively. Compared with the ideal case, with the increase of R_N, most of the points along σ^{A3} are converted to reflective, and only the points near the target point are refractive. It can be seen that the reflective region is larger than the one with σ^{A2}. When R_N decrease, all the points along σ^{A3} are still refractive. For the case with a varied C_N/L_N, the conclusion is similar to σ^{A2}, as can be seen in Fig.9(c), (d).

C. CONSIDERING PARASITIC PARAMETERS

Another noticeable non-ideal factor is the existence of parasitic parameters. When considering the parasitic resistances of the inductor and capacitor, the model of Buck converter is changed into (45), as shown at the bottom of the last page, where R_L, R_C denote the equivalent series resistance of L, C respectively. By substituting (45) into (42), the expression of the changed $\frac{d\sigma^{A2}}{dt}$ can be obtained, and the case of σ^{A3} is similar.

With different values of R_L and R_C, the effect of the parasitic parameters on the large-signal behavior is complex. Here, we only give a set of examples with typical parameters to explain this effect.

Fig.10(a) and (b) show the boundary curves of σ^{A2} and σ^{A3} with $R_L = 50m\Omega$. It can be seen that in the case of σ^{A2}, the reflective region is larger than the one in ideal case; in the case of σ^{A3}, when $u_o < U_{ref}$, the reflective region becomes larger, and when $u_o > U_{ref}$, all the points are still refractive. Moreover, it is also seen that the reflective region with σ^{A3} is larger than the one with σ^{A2} when $u_o < U_{ref}$, and R_L has the same value.

Fig.10(c) and (d) show the boundary curves of σ^{A2} and σ^{A3} with $R_C = 30m\Omega$. With σ^{A2}, a refractive region is between two reflective regions when considering $u_o < U_{ref}$ and $u_o > U_{ref}$ separately. With σ^{A3}, when $u_o < U_{ref}$, most points along the switching surface are changed to reflective; when $u_o > U_{ref}$, all the points are still refractive. Thus it can be seen the effect of R_C is relatively complicated. In general, the reflective region is enlarged due to the parasitic resistances of output capacitor.

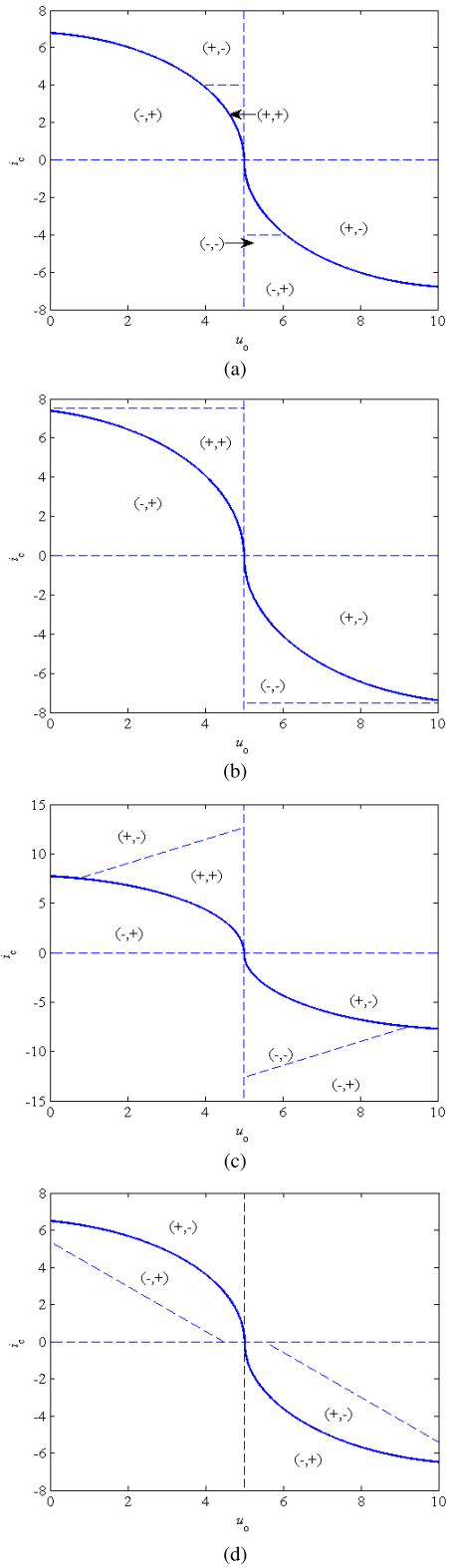

FIGURE 8. The boundary of the regions under parametric variations(σ^{A2}). (a) $R_N = 1.5R$. (b) $R_N = 0.5R$. (c) $C_N/L_N = 1.2C/L$. (d) $C_N/L_N = 0.8C/L$.

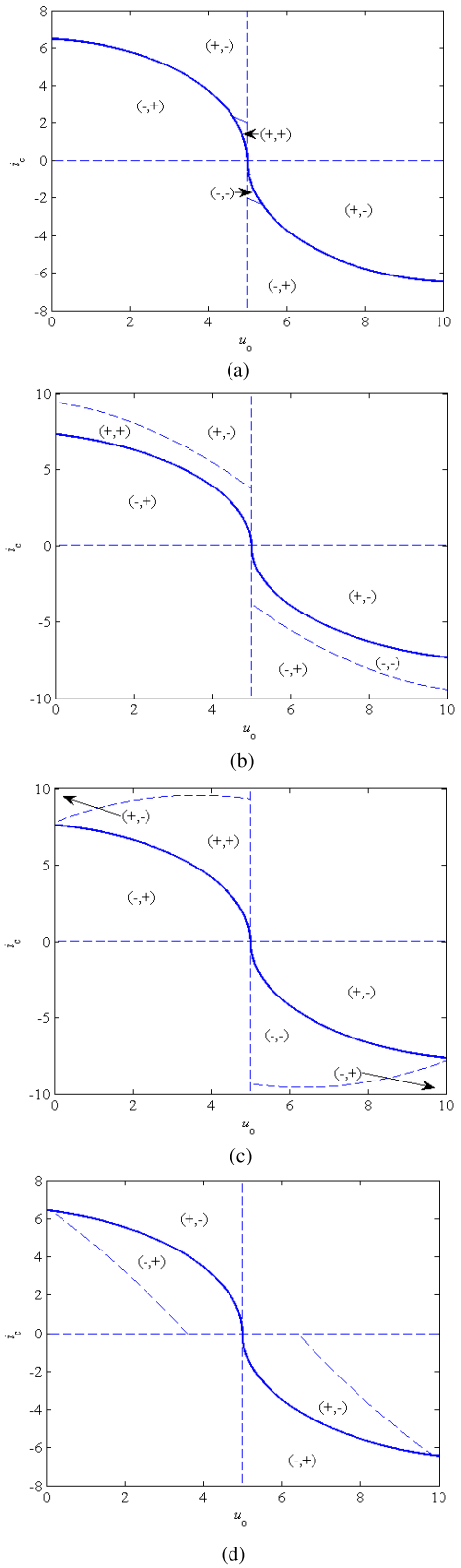

FIGURE 9. The boundary of the regions under parametric variations(σ^{A3}). (a) $R_N = 1.5R$. (b) $R_N = 0.5R$. (c) $C_N/L_N = 1.2C/L$. (d) $C_N/L_N = 0.8C/L$.

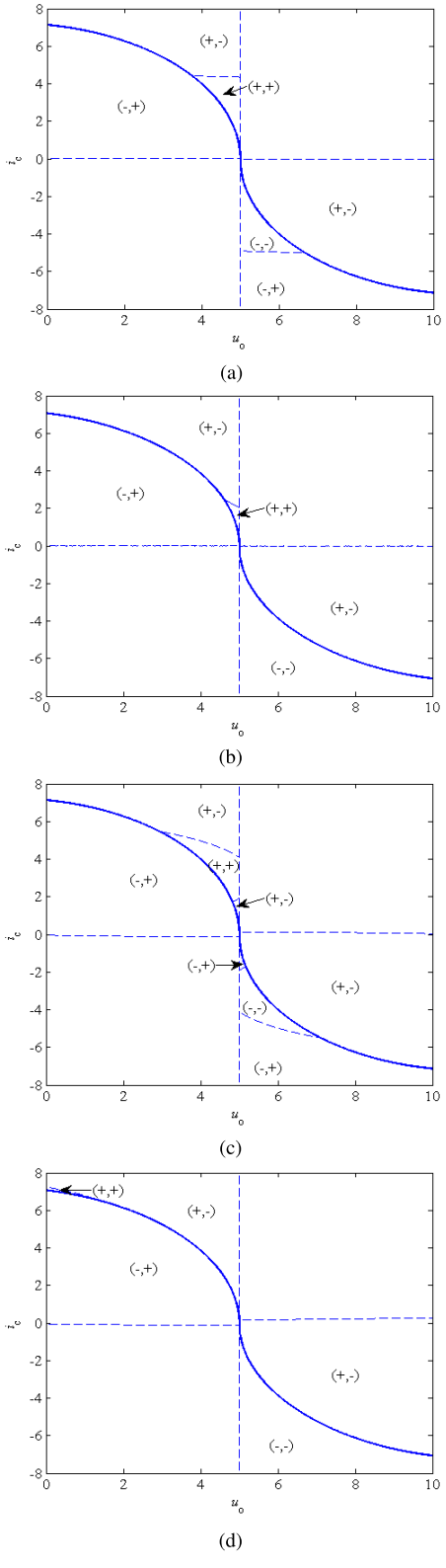

FIGURE 10. The boundary of the regions with parasitic parameters. (a) with σ^{A2} and $R_L = 50m\Omega$. (b) with σ^{A3} and $R_L = 50m\Omega$. (c) with σ^{A2} and $R_C = 30m\Omega$. (d) with σ^{A3} and $R_C = 30m\Omega$.

Fig.11 shows the simulation waveforms of startup process with σ^{A2}, $R_L = 50m\Omega$, and $R_C = 30m\Omega$. Fig.12 gives the corresponding state trajectory. Other parameters are given in Table 1. It can be seen that the overshoot voltage is eliminated completely, the state point moves along the SS strictly, and the switching

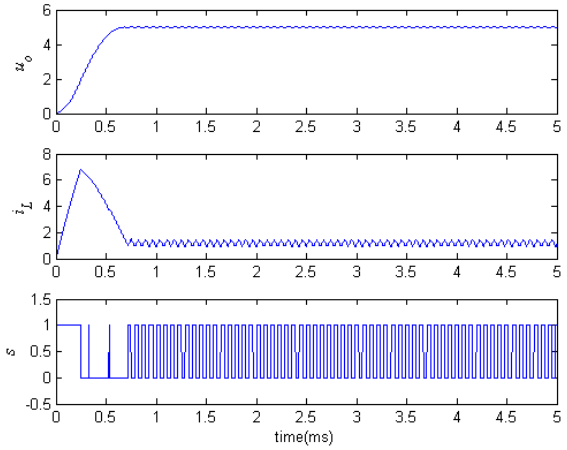

FIGURE 11. Simulation results of startup process with parasitic parameters.

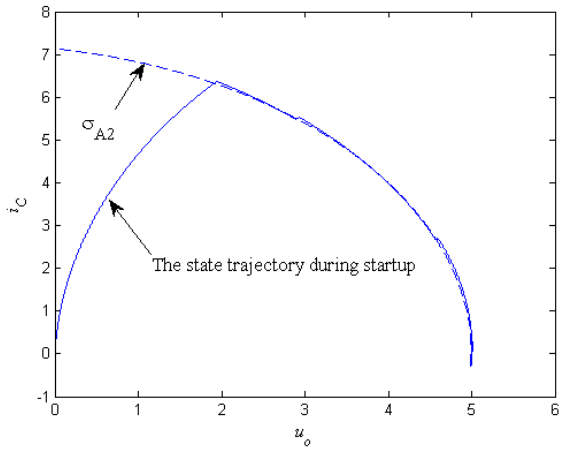

FIGURE 12. The state trajectory corresponding to Figure.11.

times are increased due to the enlargement of reflective region.

Based on above analyses, we can deduce the following information.

(1) For a specific SS, if decreasing the load resistance, the reflective region will be enlarged; otherwise the refractive region will be enlarged.

(2) For a specific SS, if decreasing the ratio of capacitance and inductance, the refractive region will be enlarged; otherwise the reflective region will be enlarged.

(3) Under the influence of the parasitic resistances, the reflective region is enlarged generally. In particular, the reflective region with σ^{A3} is larger than the one with σ^{A2} when $u_o < U_{ref}$.

IV. EXPERIMENTAL VERIFICATIONS

In order to further verify the correctness of the above theoretical results, a Buck converter prototype was built and tested with $U_{in} = 10V$ and $U_{ref} = 5V$. The power converter consists of the following components:

1) switching device: IRF8788;

2) freewheeling diode: SS10P4 ($U_D = 0.41V$);

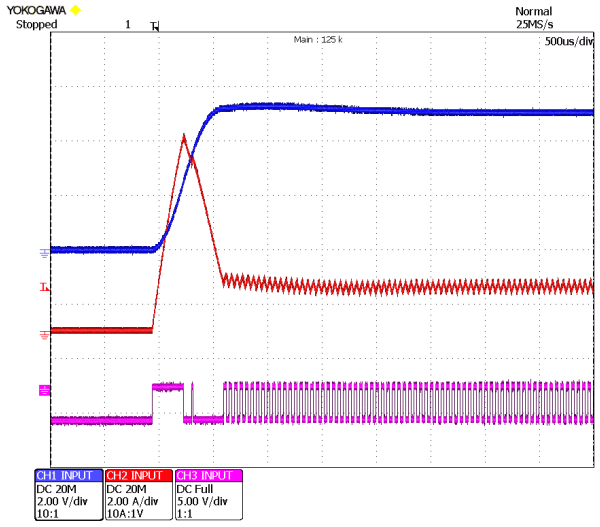

FIGURE 13. Experimental results of startup process with σ^{A2} and rated parameters [Ch.1: output voltage, Ch.2: inductor current, Ch.3: switching signal].

3) filter inductor L: $330\mu H$;

4) filter capacitor C: $480\mu F$;

5) load resistor R: 3Ω.

If not specifically mentioned, the output capacitors are composed of ten $47\mu F$ low ESR polymer tantalum capacitors and a $10\mu F$ ceramic capacitor. A $10\,m\Omega$ precise resistor is in series with the capacitor for sensing i_C. The hybrid method in [20] combining the boundary control and PWM strategy is used in the experiment. By this method, the PWM mode is adopted in the steady state, and the boundary control is activated only during the large-signal recovery process. The control law is implemented by a TMS320F28335 floating-point DSP, with which the sampling of variables and the computation of switching functions are performed at 300kHz. The internal A/D converters have 12-bit resolution and an input voltage range from 0 to 3.3 V.

A. THE CASE WITH $R_N = R$ AND $C_N/L_N = C/L$

Firstly, we give the results of the case with $R_N = R$ and $C_N/L_N = C/L$. The dynamic responses using σ^{A2} and σ^{A3} in the startup process are shown in Figs.13-14.

Fig.13 shows the case with σ^{A2}. It can be seen that the transient process is almost optimal, and the output voltage achieves the reference value with nearly no overshoot. Compared with the simulation results in Fig.4(a), there exists an extra switching action in Fig.13. This difference indicates that the reflective region is enlarged in the practical system. It is caused by the non-ideal factors of the experimental circuit, such as the existence of parasitic parameters and sampling resistors. Thus it can be seen that the sliding-mode motion will help to improve the dynamic response in the case of large deviations. Fig.14 shows the case with σ^{A3}. It can be seen that the transient response is very similar to the case with σ^{A2}.

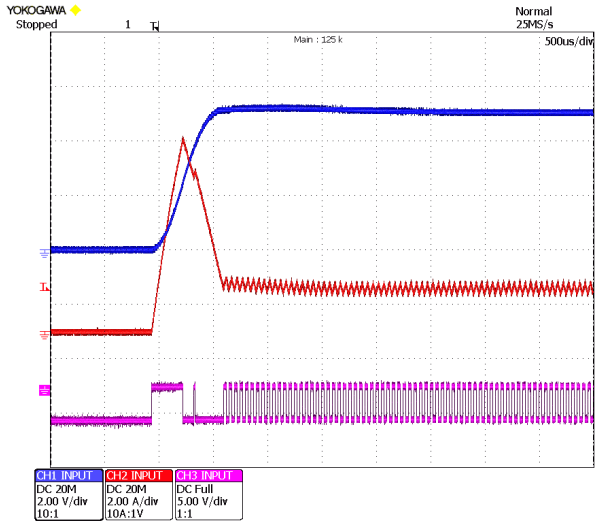

FIGURE 14. Experimental results of startup process with σ^{A3} and rated parameters [Ch.1: output voltage, Ch.2: inductor current, Ch.3: switching signal].

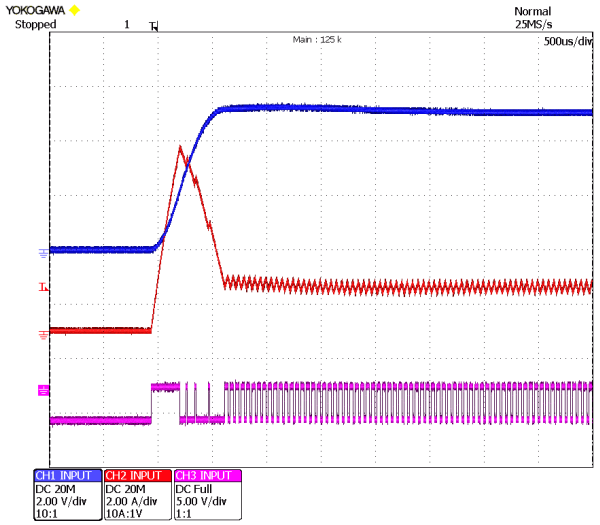

FIGURE 15. Experimental results of startup process with σ^{A2} and $R < R_N$ [Ch.1: output voltage, Ch.2: inductor current, Ch.3: switching signal].

B. THE CASE WITH $R_N \neq R$

According to the analysis in Section VI, when $R_N > R$, the reflective region will be enlarged, or else the refractive region will be enlarged. Fig.15 shows the experimental results with σ^{A2}, $R = 3\Omega$ and $R_N = 10\Omega$. It can be seen that the dynamic performance is still close to time-optimal, only the sliding-mode motion lasts longer compared with the case in Fig.13. Fig.16 shows the case with $R = 3\Omega$ and $R_N = 1\Omega$. In this case, the output voltage has a significant overshoot, which means that the system trajectory has diverged from the SS seriously. The reason for this result is the enlargement of the refractive region. The experimental results are consistent with the theoretical analyses in Fig.8.

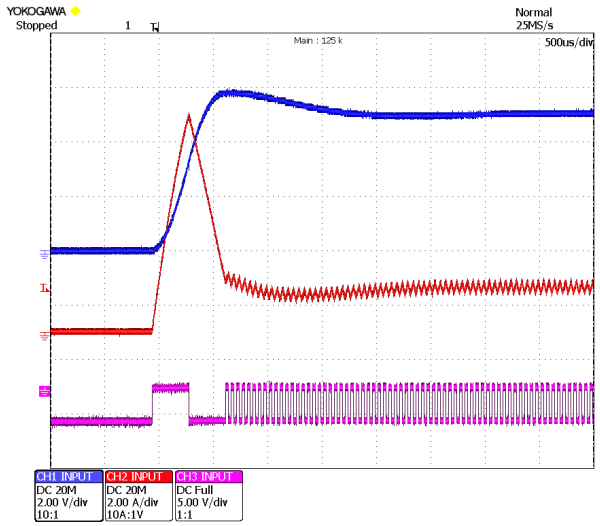

FIGURE 16. Experimental results of startup process with σ^{A2} and $R > R_N$ [Ch.1: output voltage, Ch.2: inductor current, Ch.3: switching signal].

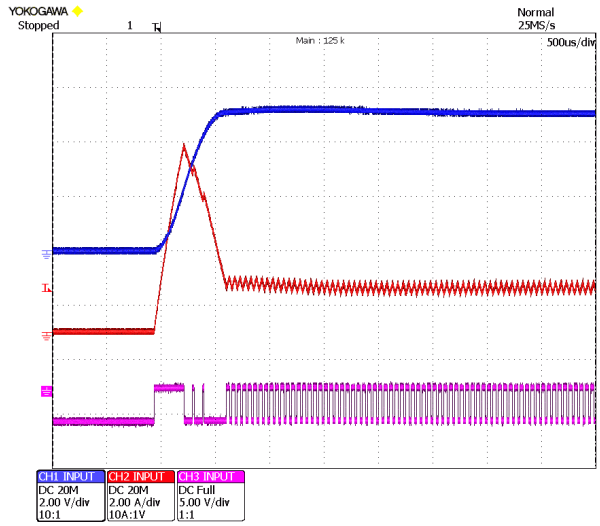

FIGURE 17. Experimental results of startup process with σ^{A2} and $C_N/L_N < C/L$ [Ch.1: output voltage, Ch.2: inductor current, Ch.3: switching signal].

C. THE CASE WITH $C_N/L_N \neq C/L$

The experimental results with $C_N/L_N \neq C/L$ are given in Figs.17-18. Fig.17 shows the results with σ^{A2}, $C = 480\mu F$ and $C_N = 384\mu F$. It can be seen that the duration time in sliding-mode region is longer, which is similar to the case in Fig.15. Fig.18 shows the results with σ^{A2}, $C = 480\mu F$ and $C_N = 576\mu F$. Accordingly, the output voltage has a significant overshoot, which is similar to the case in Fig.16. These results are also consistent with the theoretical analyses in Fig.8.

D. THE CASE WITH ELECTROLYTIC CAPACITOR

To verify the effect of parasitic resistances, we use a $470\mu F$ aluminum electrolytic capacitor, which has a larger ESR,

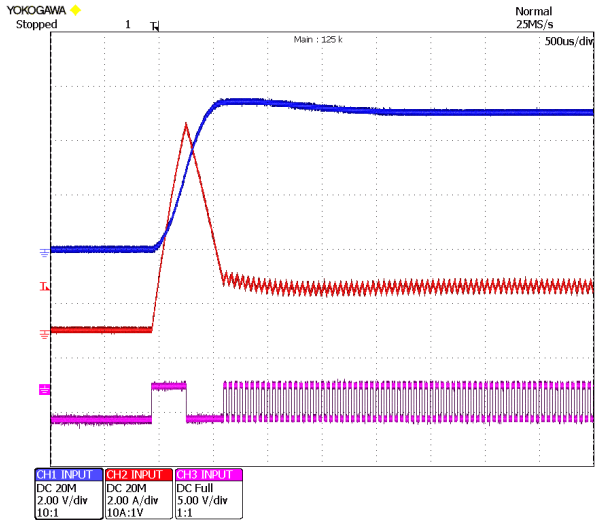

FIGURE 18. Experimental results of startup process with σ^{A2} and $C_N/L_N > C/L$ [Ch.1: output voltage, Ch.2: inductor current, Ch.3: switching signal].

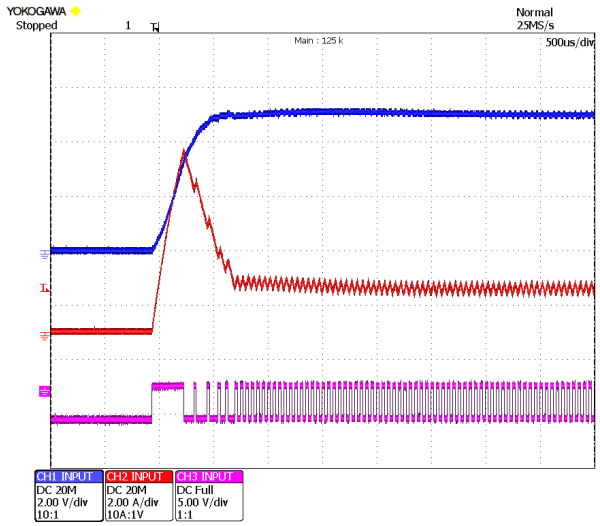

FIGURE 19. Experimental results of startup process with σ^{A2} and electrolytic capacitor [Ch.1: output voltage, Ch.2: inductor current, Ch.3: switching signal].

to replace the polymer tantalum capacitors. Fig.19 shows the experimental results with σ^{A2}, $R_N = R$ and $C_N/L_N = C/L$, and Fig.20 shows the corresponding state trajectory. It can be seen that there only exists the sliding-mode motion after the system states reach the SS. These results are consistent with the theoretical analyses in Fig.10 and the simulation results in Figs.11-12.

E. A BRIEF SUMMARY

According to the above experimental results, all the theoretical results obtained in Section III are verified, and the excellent dynamic performance of boundary control with curved SSs is shown again. Based on the above results, some principles in designing the SS can be concluded:

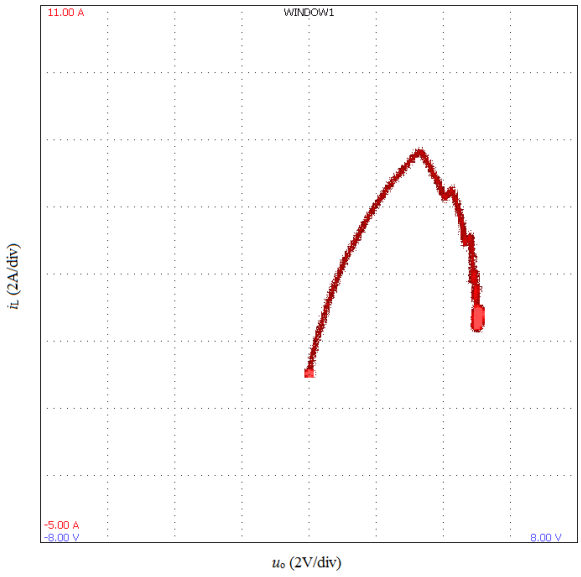

FIGURE 20. Experimental result of the state trajectory corresponding to Figure.19.

(1) The load resistance is usually unknown in practical application. To ensure the reflective region is large enough and avoid the voltage overshoot in Fig.16, the resistance value in the coefficients (R_N) should not be lower than the true value. Actually, R_N can be set as the possible maximum value. For light load application, $1/R_N = 0$ can be directly applied. That is corresponding to the case discussed in [11].

(2) For the setting of C_N/L_N, the possible parameter variations of inductance and capacitance should be considered. To avoid the voltage overshoot in Fig.18, C_N/L_N can be set as the possible minimum value with the consideration of capacitance reduction.

(3) According to the theoretical and experimental results, the parasitic resistances of inductors and capacitors will enlarge the reflective region generally, and they have no obvious negative effect on the dynamic performance. Thus, for the parasitic parameters, the effects on efficiency and voltage ripples should be taken into main consideration in practical design.

(4) Comparing the results in Fig.13 and Fig.14, it can be seen that the dynamic responses with σ^{A2} and σ^{A3} show little difference. It indicates that the second-order SS is accurate enough to provide a time-optimal dynamic response, as long as the reflective region is large enough. A higher order approximation of the ideal SS makes little sense to improve the dynamic performance. Furthermore, it will bring more difficulty in practical implementation.

V. CONCLUSION

In this paper, the influence of non-ideal factors on the boundary control of Buck converters with different SSs is analysed in detail and some design guidelines are proposed. The conclusions are listed as follows.

(1) A general expression of curved SSs with different degrees has been obtained by using the Adomian decomposition method. This expression gives an extension of the existing second-order SSs.

(2) For a specific SS, the high load resistance and low ratio of capacitance and inductance will enlarge the refractive region. This enlargement may cause a significant overshoot of the output voltage. In the determination of SS coefficients, the nominal parameters of resistance and capacitance can be set as the possible maximum and minimum value, respectively.

(3) The parasitic resistances of filter inductors and capacitors have no obvious negative effect on the dynamic performance.

(4) The higher truncation order of SS has limited effect to improve the dynamic performance. In practical application, the second-order SS is enough for obtaining a time-optimal dynamic response.

REFERENCES

[1] R. Munzert and P. T. Krein, "Issues in boundary control [of power convertors]," in *Proc. 27th Annu. IEEE Power Electron. Spec. Conf.*, Baveno, Italy, vol. 1, Jun. 1996, pp. 810–816.

[2] M. Greuel, R. Muyshondt, and P. T. Krein, "Design approaches to boundary controllers," in *Proc. Rec. 28th Annu. IEEE Power Electron. Spec. Conf.*, Saint Louis, MO, USA, vol. 1, Jun. 1997, pp. 672–678.

[3] S.-C. Tan, Y. M. Lai, M. K. H. Cheung, and C. K. Tse, "On the practical design of a sliding mode voltage controlled buck converter," *IEEE Trans. Power Electron.*, vol. 20, no. 2, pp. 425–437, Mar. 2005.

[4] S.-C. Tan, Y. M. Lai, C. K. Tse, and M. K. H. Cheung, "Adaptive feedforward and feedback control schemes for sliding mode controlled power converters," *IEEE Trans. Power Electron.*, vol. 21, no. 1, pp. 182–192, Jan. 2006.

[5] C.-C. Fang and R. Redl, "Switching frequency determination of DC–DC converters with hysteretic control," *IEEE Trans. Power Electron.*, vol. 33, no. 3, pp. 2723–2729, Mar. 2018.

[6] W. W. Burns and T. G. Wilson, "State trajectories used to observe and control DC-to-DC converters," *IEEE Trans. Aerosp. Electron. Syst.*, vol. AES-12, no. 6, pp. 706–717, Nov. 1976.

[7] W. W. Burns and T. G. Wilson, "A state-trajectory control law for DC-to-DC converters," *IEEE Trans. Aerosp. Electron. Syst.*, vol. AES-14, no. 1, pp. 2–20, Jan. 1978.

[8] K. K. S. Leung and H. S. H. Chung, "Derivation of a second-order switching surface in the boundary control of buck converters," *IEEE Power Electron Lett.*, vol. 2, no. 2, pp. 63–67, Jun. 2004.

[9] K. S. Leung and H. S. H. Chung, "A comparative study of the boundary control of buck converters using first- and second-order switching surfaces -part I: Continuous conduction mode," in *Proc. IEEE 36th Power Electron. Spec. Conf.*, Recife, Brazil, Jun. 2005, pp. 2133–2139.

[10] K. K. S. Leung and H. S. H. Chung, "A comparative study of the boundary control of Buck converters using first- and second-order switching surfaces -part II: Discontinuous conduction mode," in *Proc. IEEE 36th Power Electron. Spec. Conf.*, Recife, Brazil, Jun. 2005, pp. 2126–2132.

[11] M. Ordonez, M. T. Iqbal, and J. E. Quaicoe, "Selection of a curved switching surface for buck converters," *IEEE Trans. Power Electron.*, vol. 21, no. 4, pp. 1148–1153, Jul. 2006.

[12] M. J. Jafarian and J. Nazarzadeh, "Time-optimal sliding-mode control for multi-quadrant buck converters," *IET Power Electron.*, vol. 4, no. 1, pp. 143–150, Jan. 2011.

[13] G. E. Pitel and P. T. Krein, "Trajectory paths for DC–DC converters and limits to performance," in *Proc. IEEE Workshops Comput. Power Electron.*, Troy, NY, USA, Jul. 2006, pp. 40–47.

[14] G. Feng, E. Meyer, and Y.-F. Liu, "A new digital control algorithm to achieve optimal dynamic performance in DC-to-DC converters," *IEEE Trans. Power Electron.*, vol. 22, no. 4, pp. 1489–1498, Jul. 2007.

[15] E. Meyer and Y.-F. Liu, "A practical minimum time control method for buck converters based on capacitor charge balance," in *Proc. 23rd Annu. IEEE Appl. Power Electron. Conf. Expo.*, Feb. 2008, pp. 10–16.

[16] V. Yousefzadeh, A. Babazadeh, B. Ramachandran, E. Alarcon, L. Pao, and D. Maksimovic, "Proximate time-optimal digital control for synchronous buck DC–DC converters," *IEEE Trans. Power Electron.*, vol. 23, no. 4, pp. 2018–2026, Jul. 2008.

[17] W.-T. Yan, C. N.-M. Ho, H. S.-H. Chung, and K. T. K. Au, "Fixed-frequency boundary control of buck converter with second-order switching surface," *IEEE Trans. Power Electron.*, vol. 24, no. 9, pp. 2193–2201, Sep. 2009.

[18] L. Corradini, A. Babazadeh, A. Bjeletić, and D. Maksimović, "Current-limited time-optimal response in digitally controlled DC–DC converters," *IEEE Trans. Power Electron.*, vol. 25, no. 11, pp. 2869–2880, Nov. 2010.

[19] L. Corradini, A. Costabeber, P. Mattavelli, and S. Saggini, "Parameter-independent time-optimal digital control for point-of-load converters," *IEEE Trans. Power Electron.*, vol. 24, no. 10, pp. 2235–2248, Oct. 2009.

[20] S. Kapat and P. T. Krein, "Improved time optimal control of a buck converter based on capacitor current," *IEEE Trans. Power Electron.*, vol. 27, no. 3, pp. 1444–1454, Mar. 2012.

[21] T.-T. Song and H. S.-H. Chung, "Boundary control of boost converters using state-energy plane," *IEEE Trans. Power Electron.*, vol. 23, no. 2, pp. 551–563, Mar. 2008.

[22] J. M. Galvez, M. Ordonez, F. Luchino, and J. E. Quaicoe, "Improvements in boundary control of boost converters using the natural switching surface," *IEEE Trans. Power Electron.*, vol. 26, no. 11, pp. 3367–3376, Nov. 2011.

[23] J. Y.-C. Chiu, K. K.-S. Leung, and H. S.-H. Chung, "High-order switching surface in boundary control of inverters," *IEEE Trans. Power Electron.*, vol. 22, no. 5, pp. 1753–1765, Sep. 2007.

[24] M. Ordonez, J. E. Quaicoe, and M. T. Iqbal, "Advanced boundary control of inverters using the natural switching surface: Normalized geometrical derivation," *IEEE Trans. Power Electron.*, vol. 23, no. 6, pp. 2915–2930, Nov. 2008.

[25] S. Chen, Y. M. Lai, S.-W. Tan, and C. K. Tse, "Boundary control with ripple-derived switching surface for DC–AC inverters," *IEEE Trans. Power Electron.*, vol. 24, no. 12, pp. 2873–2885, Dec. 2009.

[26] P. K. W. Chan, H. S.-H. Chung, and S. Y. Hui, "A generalized theory of boundary control for a single-phase multilevel inverter using second-order switching surface," *IEEE Trans. Power Electron.*, vol. 24, no. 10, pp. 2298–2313, Oct. 2009.

[27] J. M. Galvez and M. Ordonez, "High performance boundary control of boost-derived PFCs: Natural switching surface derivation and properties," *IEEE Trans. Power Electron.*, vol. 27, no. 8, pp. 3807–3816, Aug. 2012.

[28] G. G. Oggier and M. Ordonez, "Boundary control of full-bridge ZVS: Natural switching surface for transient and steady-state operation," *IEEE Trans. Ind. Electron.*, vol. 61, no. 2, pp. 969–979, Feb. 2014.

[29] G. G. Oggier, M. Ordonez, J. M. Galvez, and F. Luchino, "Fast transient boundary control and steady-state operation of the dual active bridge converter using the natural switching surface," *IEEE Trans. Power Electron.*, vol. 29, no. 2, pp. 946–957, Feb. 2014.

[30] J. Ge, Z. Zhao, L. Yuan, T. Lu, and F. He, "Direct power control based on natural switching surface for three-phase PWM rectifiers," *IEEE Trans. Power Electron.*, vol. 30, no. 6, pp. 2918–2922, Jun. 2015.

[31] Y. He, H. S.-H. Chung, C. N.-M. Ho, and W. Wu, "Use of boundary control with second-order switching surface to reduce the system order for deadbeat controller in grid-connected inverter," *IEEE Trans. Power Electron.*, vol. 31, no. 3, pp. 2638–2653, Mar. 2016. doi: 10.1109/TPEL.2015.2441117.

[32] Y. He, H. S.-H. Chung, C. N.-M. Ho, and W. Wu, "Direct current tracking using boundary control with second-order switching surface for three-phase three-wire grid-connected inverter," *IEEE Trans. Power Electron.*, vol. 32, no. 7, pp. 5723–5740, Jul. 2017.

[33] G. Adomian, "A review of the decomposition method in applied mathematics," *J. Math. Anal. Appl.*, vol. 135, no. 2, pp. 501–544, Nov. 1988.

[34] G. Gurrala, D. L. Dinesha, A. Dimitrovski, P. Sreekanth, S. Simunovic, and M. Starke, "Large multi-machine power system simulations using multi-stage Adomian decomposition," *IEEE Trans. Power Syst.*, vol. 32, no. 5, pp. 3594–3606, Sep. 2017.

[35] R. Rach, "A convenient computational form for the Adomian polynomials," *J. Math. Anal. Appl.*, vol. 102, no. 2, pp. 415–419, Sep. 1984.

[36] A.-M. Wazwaz, "A reliable modification of Adomian decomposition method," *Appl. Math. Comput.*, vol. 102, no. 1, pp. 77–86, Jul. 1999.

JINGHAO LI was born in China, in 1990. He received the bachelor's degree in electrical engineering from Tianjin Polytechnic University, Tianjin, China, in 2013, and the master's degree in electrical engineering from North China Electric Power University, Beijing, China, in 2016. He is currently pursuing the Ph.D. degree with Tianjin University.

His research interest includes nonlinear control technology of power electronic converters.

AIGUO WU was born in China, in 1954. He received the bachelor's and master's degrees in automation control from Tianjin University, Tianjin, China, in 1982 and 1987, respectively.

Since 1982, he has been with the Department of Automation, Tianjin University, where he is currently a Professor and the Director of the Tianjin University-Honeywell Building Automation Center. From 2002 to 2015, he was the Dean of the Department of Automation, Tianjin University. Since 2015, he has been the Associate Director of the Academic Committee with the School of Electrical and Information Engineering, Tianjin University. He is the author of over 100 articles and one book. His research interests include power electronic converters and systems, mechanical and hydraulic nonlinear control systems, intelligent building, modeling and control of refrigeration systems, and automatic control systems for chemical process.

Prof. Wu is a member of the Technical Committee on Application of the Chinese Association of Automation. He was a recipient of the 1998 Science and Technology Progress Award presented by the Ministry of Education, and the Tianjin Science and Technology Progress Award, in 2009.